From one cell to the whole froth: A dynamical map

T. Aste,* D. Boosé, and N. Rivier
Laboratoire de Physique Théorique, Université Louis Pasteur, F 67084 Strasbourg Cedex, France
(Received 24 July 1995; revised manuscript received 14 December 1995)

We investigate two- and three-dimensional shell-structured-inflatable froths, which can be constructed by a recursion procedure adding successive layers of cells around a germ cell. We prove that any froth can be reduced into a system of concentric shells. There is only a restricted set of local configurations for which the recursive inflation transformation is not applicable. These configurations are inclusions between successive layers and can be treated as vertices and edges decorations of a shell-structured-inflatable skeleton. The recursion procedure is described by a logistic map, which provides a natural classification into Euclidean, hyperbolic, and elliptic froths. Froths tiling manifolds with different curvatures can be classified simply by distinguishing between those with a bounded or unbounded number of elements per shell, without any *a priori* knowledge on their curvature. A result, associated with maximal orientational entropy, is obtained on topological properties of natural cellular systems. The topological characteristics of all experimentally known tetrahedrally close-packed structures are retrieved.

PACS number(s): 82.40.Ck, 82.70.Rr

I. INTRODUCTION

A froth is a (topologically stable) division of space by cells, which are convex polytopes [polygons in two-dimensions (2D), polyhedra in three dimensions (3D)] of various shapes and sizes. These geometrical systems have attracted much attention in recent years, both theoretically and experimentally [1,2]. The aim in this work is to study a specific class of froths, namely, those which are reducible to a set of concentric shells. These particular froths are structured as if constructed in the following way. In the first stage, cells are added to a germ cell, forming a first layer around it whose external surface constitutes the second shell. In the second stage, cells are added to the first shell so as to form a second layer of cells encircling the first one, and so on. We emphasize that the words ''germ'' and ''stage'' are purely pictorial and do not imply any particular mode of growth since any cell of a generic shell-structured froth may play the role of its germ cell. Such a froth is called shell-structured inflatable from now on.

A definition of a shell-structured-inflatable froth requires the notion of a topological distance between cells. The topological distance t between two cells A and B is defined as the smallest number of edges crossed by a path connecting A and B. The germ cell is therefore at the distance $t=0$. A shell (t) is defined as the interface between two sets of cells distant by t and $t+1$ from the germ cell. A 2D froth is a *shell-structured inflatable* froth if it satisfies the following two conditions:

(1) For any set of cells, equidistant to the germ cell, there exists a closed non-self-intersecting path which goes only through these cells and connects all of them.

(2) Any cell at distance t from the germ cell is the neighbor of at least one cell at the distance $t+1$.

Two consecutive shells (t) and $(t+1)$ of a shell-structured-inflatable froth are connected through a set of disjoint edges with one vertex on shell (t) and the other on shell $(t+1)$. These two shells are closed loops of edges delimiting the layer $(t+1)$ of cells which are at the distance $t+1$ from the germ cell. Shell (t) divides the froth into an internal froth, constituted of cells at distances $r \leqslant t$, and an external froth, with cells at distances $r>t$. The extension to 3D shell-structured-inflatable froths is straightforward and is given in Appendix B 2.

In this paper we prove that the 2D and 3D shell-structured-inflatable froths are constructed according to a recursion procedure which is the logistic map [3], well known in the theory of dynamical systems. The logistic map provides a natural classification of these froths according to the behavior of the number of edges per shell as the topological distance t increases.

Any given froth is not necessarily shell-structured inflatable. However, it has to be noted that a froth can always be decomposed into shells with respect to an arbitrarily chosen germ cell. In this decomposition, each cell of the layer (t) belongs to one of two categories. The cells of the first category, individually, have neighbors in both layers $(t-1)$ and $(t+1)$ and, collectively, are building up a complete ring around the chosen germ cell. The set of all these rings constitutes the ''skeleton'' of the shell structure. The cells of the second category have neighbors in only one of the two layers $(t-1)$ or $(t+1)$. These cells can be considered as local topological defects included between the rings of the ''skeleton'' of the shell structure. The ''skeleton'' is itself a space-filling froth which is shell-structured inflatable. The recursion procedure that we are studying applies to such a structure.

The plan of this paper is the following. In Sec. II, we derive the recursion procedure associated with 2D shell-structured-inflatable froths and show that it can be written as the logistic map. The resulting classification into Euclidean, hyperbolic, and elliptic froths is discussed. In Sec. III, it is shown that the recursion procedure in 3D is again described

*On leave from C.I.I.M., Universitá di Genova, Genova, Italy.

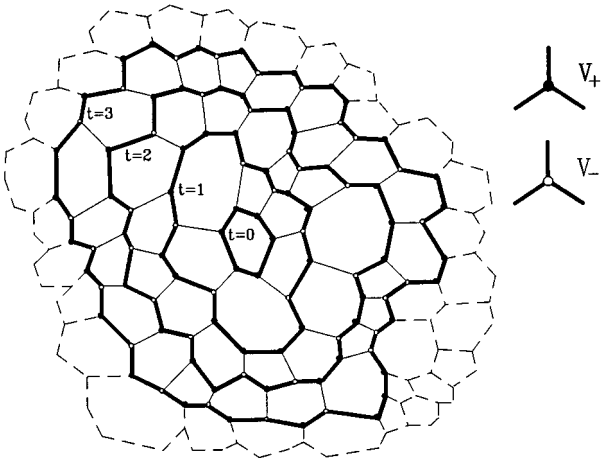

FIG. 1. Schematic picture of a 2D shell-structured-inflatable froth.

by a logistic map. The curvature of the embedding space is classified as for the 2D froths. Section IV gives examples of space-filling cellular structures which fit into the classification of 3D shell-structured-inflatable froths provided by the logistic map. In Sec. V, a bound on topological properties of natural cellular structures is obtained. The topological properties of all experimentally known tetrahedrally close-packed (t.c.p.) structures are retrieved under the hypothesis of shell reducibility. A conclusion emphasizes the main results of the paper. In Appendix A, the recursion procedure is generalized to 2D shell-structured-inflatable networks with a vertex coordination larger than three. Local topological defects in 2D and 3D shell-reducible but not inflatable froths are considered in Appendix B. Random 3D Euclidean froths are constructed from 2D random shell networks in Appendix C.

II. RECURSION PROCEDURE FOR 2D FROTHS

This section is concerned with two-dimensional shell-structured-inflatable froths. The recursion procedure is derived here for froths and it is extended to networks with a vertex coordination larger than three in Appendix A. Figure 1 shows an example of a froth with the various shells indicated by bold lines and labeled by the index t (the shell $t=0$ corresponding to the boundary of the germ cell). Let $V_{+(-)}^{(t)}$ be the number of vertices going out from shell (t) towards shell $(t+1)$ [towards shell $(t-1)$]. Let $F^{(t)}$ be the number of cells in the layer between shells (t) and $(t+1)$. If $\langle n\rangle$ is the average number of edges per cell in layer (t), the edges in this layer are accounted for, as follows:

$$\langle n\rangle F^{(t)}=V_{-}^{(t)}+2V_{+}^{(t)}+2V_{-}^{(t+1)}+V_{+}^{(t+1)}. \tag{2.1}$$

In the right-hand side of this equation, the quantity $V_{-}^{(t)}+V_{+}^{(t)}$ is the total number of vertices constituting shell (t), the quantity $V_{-}^{(t+1)}+V_{+}^{(t+1)}$ is the total number of vertices constituting shell $(t+1)$ whereas the quantity $V_{-}^{(t+1)}+V_{+}^{(t)}$ gives the number of vertices (counted twice) bounding the edges separating the cells comprised between shells (t) and $(t+1)$. Since $V_{+}^{(t)}=V_{-}^{(t+1)}$ and $F^{(t)}=V_{+}^{(t)}$, one has the recursion equation

$$\langle n\rangle V_{+}^{(t)}=4V_{+}^{(t)}+V_{+}^{(t+1)}+V_{-}^{(t)}. \tag{2.2}$$

The matrix form of this recursion equation is

$$\begin{pmatrix} V_{+}^{(t+1)} \\ V_{-}^{(t+1)} \end{pmatrix}=\begin{pmatrix} s & -1 \\ 1 & 0 \end{pmatrix}\begin{pmatrix} V_{+}^{(t)} \\ V_{-}^{(t)} \end{pmatrix}, \tag{2.3}$$

with the recursion parameter $s=\langle n\rangle-4$. Equation (2.3) generates recursively the whole froth from the germ cell. In general, the quantity $\langle n\rangle$ changes from one layer to the next. Hence the recursion parameter should depend on the distance t. However, the value of $\langle n\rangle$ associated to a layer of cells at a distance t from the germ cell must, as $t\to\infty$, converge to the average value for any cell in the froth. Moreover, since the choice of the germ cell is completely arbitrary, the quantity $\langle n\rangle$ associated with layer (t) is an average. Consequently, the recursion parameter can be taken as an effective quantity which is independent of t, and the quantity $\langle n\rangle$ is then the average number of edges per cell in the froth. The initial conditions in Eq. (2.3) are then $V_{-}^{(0)}=0$ and $V_{+}^{(0)}=\langle n\rangle$.

The recursion procedure described in Eq. (2.3) appears also in other instances, such as in the computation by decimation of the electronic energy spectrum in the 1D tight-binding model [4]. In this case, the variables $V^{(t)}$ are replaced by the components of the electronic wave functions in the basis of the site states, and the recursion parameter s is the (dimensionless) energy of the electron.

Equation (2.3) gives an immediate link between the shell-structured-inflatable froths and the logistic map. Indeed, from the relations $sV_{+}^{(t)}=V_{+}^{(t+1)}+V_{+}^{(t-1)}$, $sV_{+}^{(t+1)}=V_{+}^{(t+2)}+V_{+}^{(t)}$, and $sV_{+}^{(t-1)}=V_{+}^{(t)}+V_{+}^{(t-2)}$, one gets

$$s_1V_{+}^{(t)}=V_{+}^{(t+2)}+V_{+}^{(t-2)}, \tag{2.4}$$

with

$$s_1=s^2-2, \tag{2.5}$$

and a similar relation for V_{-}. Iterating j times, one obtains

$$s_jV_{+}^{(t)}=V_{+}^{(t+2^j)}+V_{+}^{(t-2^j)}, \tag{2.6}$$

with

$$s_{j+1}=s_j^2-2, \tag{2.7}$$

and $s_0=s$. Equation (2.7) is the trace map of the recursion matrix in Eq. (2.3). It is a logistic map [3], with two (unstable) fixed points $s^*=2$ and $s^*=-1$. The logistic map decomposes the axis of values of the recursion parameter s into two different regions. Any point in the region $|s|>2$ is sent towards infinity by the successive iterations of the logistic map. By contrast, if $|s|<2$, successive iterations of the logistic map remain all within this interval. The existence of these two intervals classifies all 2D shell-structured-inflatable froths. This classification corresponds to the curvature of the manifold which the froth tiles. The space is elliptic for $|s|<2$, hyperbolic for $|s|>2$, and Euclidean for the fixed point $s=s^*=2$. The map relates successive numbers $V^{(t)}$ of vertices per shell. Iterations of Eq. (2.3) generate

trajectories in the plane (t,V_+), starting from the initial points $V_+^{(-1)}=V_-^{(0)}=0$ and $V_+^{(0)}=\langle n\rangle$.

When $|s|<2$, the trajectories are given by the equation

$$V_+^{(t)}=V_+^{(0)}\frac{\sin[\varphi(t+1)]}{\sin\varphi}, \tag{2.8}$$

with $\cos(\varphi)=s/2$. Equation (2.8) shows that all trajectories are finite and end at the point $V_+^{(T)}=0$, with $T=(\pi/\varphi)-1$. Moreover, the values of $V_+^{(t)}$ are bounded by the quantity $V_+^{(0)}/\sin(\varphi)$. These finite and bounded trajectories are describing the iterative tiling of the compact manifolds with a positive curvature. Indeed, consider a froth tiling the surface of a sphere. Suppose that the north pole of the sphere is located in the germ cell; the successive shells are the parallels on the sphere. The number of vertices per shell increases between the north pole and the equator, then decreases from the equator to the south pole where the tiling ends. This is precisely the behavior described by Eq. (2.8). The quantity $T+1=\pi/\varphi$ is the topological distance between both poles. Here are a few examples of regular froths with $|s|<2$. To $s=-1$ corresponds a froth made with four triangles, i.e., the surface of a tetrahedron. The recursion parameter $s=0$ corresponds to a froth made with six squares, i.e., the surface of a cube. Finally $s=1$ is associated with a froth which is the surface of a dodecahedron.

In the case $|s|>2$, the solution of Eq. (2.3) is

$$V_+^{(t)}=V_+^{(0)}\frac{\sinh[\varphi(t+1)]}{\sinh\varphi}, \tag{2.9}$$

with $\cosh(\varphi)=s/2$. Equation (2.9) shows that, contrary to the previous case, the values of $V_+^{(t)}$ increase exponentially with t. All trajectories are now infinite and unbounded in the plane (t,V_+). They are therefore describing the iterative tiling of the noncompact manifolds with a negative curvature.

At the fixed point $s=s^*=2$, Eq. (2.3) has the solution

$$V_+^{(t)}=(t+1)V_+^{(0)}. \tag{2.10}$$

The values of $V_+^{(t)}$ have again no upper bound, but here they are increasing linearly with t as expected for the Euclidean plane by simple geometrical considerations. The fixed point $s^*=2$ describes shell-structured-inflatable froths covering the Euclidean plane with cells with six edges on average. An example of such froths is the hexagonal tiling.

We have shown that the logistic map provides, in a natural way, the topological classification of the tilings of the manifolds without any *a priori* knowledge of their Gaussian curvature. In 2D this classification by the logistic map is identical to that provided by the combination of the Gauss-Bonnet theorem [5] and Euler's equation

$$\int\int \kappa\, da=\frac{\pi}{3}(6-\langle n\rangle)F=\frac{\pi}{3}(2-s)F. \tag{2.11}$$

Here, κ is the Gaussian curvature and it is integrated over the whole manifold. F is the total number of cells in the manifold. The tiled manifold is hyperbolic, Euclidean, or elliptic when the integrated curvature is negative, zero, or positive, i.e., when the recursion parameter s is larger, equal to, or smaller than two. However, the logistic map is also applicable in 3D where there is no Gauss-Bonnet theorem and the Euler equation is homogeneous [6].

III. RECURSION PROCEDURE FOR 3D FROTHS

This section extends the analysis of the previous one to 3D shell-structured-inflatable froths. The froth has V vertices, E edges, F faces, and C polyhedra. Every shell of the 3D froth is built up from two superposed different two-dimensional froths, and looks like a corrugated sphere. This is the same as in 2D, where a shell can be regarded as the superposition of two 1D froths, one whose vertices are connected to the ''incoming'' edges from shell $(t-1)$ to shell (t), and the other whose vertices are connected to the ''outgoing'' edges pointing from shell (t) towards shell $(t+1)$. Similarly, every spherical shell (t) of the 3D froth is built-up of the superposition of two 2D froths, one whose edges are connected to the ''incoming'' faces of layer $(t-1)$, and the other whose edges are connected to the ''outgoing'' faces of layer (t). Let $V_{+(-)}^{(t)}$ and $E_{+(-)}^{(t)}$ be the numbers of vertices and edges of shell (t), bounding the cells of layer (t) between shells (t) and $(t+1)$ [layer $(t-1)$ between shells (t) and $(t-1)$, respectively], which are making the ''outgoing'' (''incoming'') froth. Let $F_{+(-)}^{(t)}$ be the number of faces of such froths. Both froths are characterized by the identities

$$V_{+(-)}^{(t)}-E_{+(-)}^{(t)}+F_{+(-)}^{(t)}=2 \tag{3.1}$$

(Euler's formula) and

$$3V_{+(-)}^{(t)}=2E_{+(-)}^{(t)} \tag{3.2}$$

(since in both 2D froths, any vertex is connected by three edges and any edge is bounded by two vertices).

One has the following relations between two successive shells:

$$\begin{aligned} V_-^{(t+1)}&=V_+^{(t)},\\ E_-^{(t+1)}&=E_+^{(t)},\\ F_-^{(t+1)}&=F_+^{(t)}. \end{aligned} \tag{3.3}$$

Shell (t) is a spherical surface tiled by a network with $F_N^{(t)}$ faces. One has

$$F_N^{(t+1)}=\langle f\rangle F_+^{(t)}-2E_+^{(t)}-F_N^{(t)}. \tag{3.4}$$

In this equation, $\langle f\rangle$ is the average number of faces per cell in the layer (t).

Since the whole shell (t) is a polyhedron, both Euler's formula and the incidence relations are applicable between the number of edges $E_N^{(t)}$, the number of vertices $V_N^{(t)}$, and the number of faces $F_N^{(t)}$ of the shell polyhedron, namely,

$$V_N^{(t)}-E_N^{(t)}+F_N^{(t)}=2 \tag{3.5}$$

and

$$\langle n\rangle_N F_N^{(t)}=2E_N^{(t)}. \tag{3.6}$$

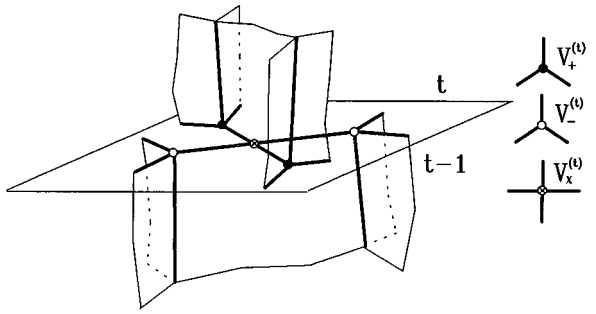

FIG. 2. Any 3D shell (t) is tiled with a network generated by the intersection of the faces coming to and going away from its surface. This shell-network has four-connected vertices $V_\times^{(t)}$ (with all four edges belonging to the shell network) and three-connected vertices $V_{+(-)}^{(t)}$ (with three edges belonging to the shell network and the last one going away from it).

Here $\langle n\rangle_N$ is the average number of edges per face of the shell polyhedron. Since it is an elliptic tiling with a vertex coordination $\geqslant 3$, then $\langle n\rangle_N < 6$. The shell network is the superposition of two 2D froths, it has therefore three-connected vertices $V_{+(-)}$ corresponding to the ''outgoing'' (''incoming'') froth, and also four-connected vertices $V_\times$ at the intersections between the edges of the two 2D froths. The three types of vertices are represented in Fig. 2. Figure 3 shows the shell network in the particular case of the ''Kelvin froth'' [7,8], and indicates a three-connected vertex and a four-connected vertex.

The total number of vertices $V_N^{(t)}$ on shell (t) is the sum of all three- and four-connected vertices, i.e.,

$$V_N^{(t)} = V_+^{(t)} + V_-^{(t)} + V_\times^{(t)}. \tag{3.7}$$

The total number of edges $E_N^{(t)}$ on shell (t) satisfies the equation

$$2E_N^{(t)} = 3V_+^{(t)} + 3V_-^{(t)} + 4V_\times^{(t)}. \tag{3.8}$$

Using Eqs. (3.5), (3.6), and (3.8), one obtains

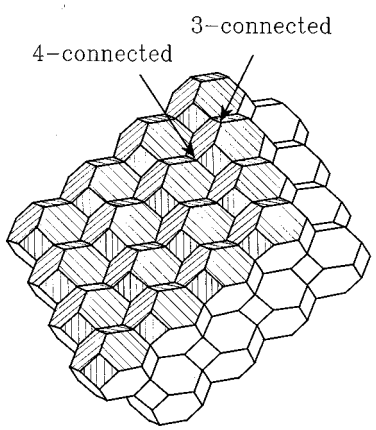

FIG. 3. An example of 3D shell-structured-inflatable froth, the Kelvin froth. A portion of the shell network is brought out by hatcheries.

$$V_N^{(t)} = 2 + \frac{1}{2}\left(1 - \frac{2}{\langle n\rangle_N}\right)(3V_+^{(t)} + 3V_-^{(t)} + 4V_\times^{(t)}). \tag{3.9}$$

Combining Eqs. (3.7) and (3.9), it is possible to express the variable $V_\times^{(t)}$ in terms of the variables $V_+^{(t)}$ and $V_-^{(t)}$ alone as

$$2V_\times^{(t)} = \frac{4\langle n\rangle_N}{4-\langle n\rangle_N} - (V_+^{(t)} + V_-^{(t)})\left(\frac{6-\langle n\rangle_N}{4-\langle n\rangle_N}\right), \tag{3.10}$$

which, with Eqs. (3.6) and (3.8), yields

$$F_N^{(t)} = \frac{8-(V_+^{(t)} + V_-^{(t)})}{4-\langle n\rangle_N}. \tag{3.11}$$

Putting Eq. (3.11) into Eq. (3.4), we obtain, with the help of Eqs. (3.1)-(3.3), the following relation:

$$V_+^{(t+1)} = \tfrac{1}{2}[(\langle f\rangle - 6)(\langle n\rangle_N - 4) - 4]V_+^{(t)} - V_-^{(t)} + 2[8 + \langle f\rangle(\langle n\rangle_N - 4)]. \tag{3.12}$$

Finally, by shifting the variables $V_{+(-)}$ as

$$\tilde{V}_{+(-)}^{(t)} = V_{+(-)}^{(t)} - 4\left(\frac{8+\langle f\rangle(\langle n\rangle_N - 4)}{8-(\langle f\rangle - 6)(\langle n\rangle_N - 4)}\right), \tag{3.13}$$

one obtains the recursion equation

$$s\tilde{V}_+^{(t)} = \tilde{V}_+^{(t+1)} + \tilde{V}_+^{(t-1)}, \tag{3.14}$$

with the recursion parameter

$$s = \tfrac{1}{2}[(\langle f\rangle - 6)(\langle n\rangle_N - 4) - 4]. \tag{3.15}$$

This recursion equation has the same matrix form as in the 2D case

$$\begin{pmatrix} \tilde{V}_+^{(t+1)} \\ \tilde{V}_-^{(t+1)} \end{pmatrix} = \begin{pmatrix} s & -1 \\ 1 & 0 \end{pmatrix} \begin{pmatrix} \tilde{V}_+^{(t)} \\ \tilde{V}_-^{(t)} \end{pmatrix}. \tag{3.16}$$

As in the 2D case $\langle f\rangle$ and $\langle n\rangle_N$ can be supposed to be independent of the distance t. The variation of the 3D recursion parameter s [the trace of the transfer matrix in Eq. (3.16)] is described by the logistic map (2.7), as in the 2D case. Consequently, the classification of the 3D shell-structured-inflatable froths is the same as in 2D.

Elliptic shell-structured-inflatable froths are associated with $|s| < 2$. They are tiling iteratively the 3D compact manifolds with a positive curvature. Indeed, the corresponding solution of Eq. (3.16) is finite and bounded in the (t,V) plane

$$V_+^{(t)} = A\ \sin(\varphi t + B) + 2\left(\frac{8+\langle f\rangle(\langle n\rangle_N - 4)}{2-s}\right), \tag{3.17}$$

with $\cos(\varphi) = s/2$. The coefficients A and B can be deduced from the initial conditions $V_+^{(0)} = 2(\langle f\rangle - 2)$ and $V_+^{(-1)} = 0$.

Hyperbolic shell-structured-inflatable froths are associated with $|s| > 2$. They are tiling iteratively 3D noncompact manifolds with a negative curvature. Indeed, the corresponding solution of Eq. (3.16) is unbounded in the (t,V) plane

$$V_+^{(t)} = A\ \sinh(\varphi t + B) + 2\left(\frac{8+\langle f\rangle(\langle n\rangle_N - 4)}{2-s}\right), \quad (3.18)$$

with $\cosh(\varphi) = s/2$. As previously, the coefficients A and B can be determined from the initial conditions.

For $s = -2$ the solution reads

$$V_+^{(t)} = (-1)^t(At + B) + \frac{8+\langle f\rangle(\langle n\rangle_N - 4)}{2}, \quad (3.19)$$

with A and B deducible from the initial conditions.

The solution of Eq. (3.16) associated to the fixed point $s = s^* = 2$ is

$$V_+^{(t)} = (t+1)\{V_+^{(0)} + t[8+\langle f\rangle(\langle n\rangle_N - 4)]\}. \quad (3.20)$$

The quadratic dependence in t is the one expected from simple geometrical reasoning for a tiling of the 3D Euclidean space.

As in 2D, the logistic map gives a natural description of the tilings of the three-dimensional manifolds without the need of any *a priori* information on their curvature. Consequently, the logistic map is able to characterize curved manifolds even when the Gauss-Bonnet formula is not applicable [9,10]. The generation of tilings of the curved manifold by the recursion procedure has therefore a wider applicability than the Gauss-Bonnet formula.

IV. EXAMPLES OF 3D SHELL-STRUCTURED-INFLATABLE FROTHS

In order to illustrate the previous considerations, we give some known examples of 3D froths and show that they fit our classification. All are monotiled (i.e., constituted of topologically identical cells), apart from the last example.

The only regular elliptic froths in 3D are {3,3,3} (packing of tetrahedra), {4,3,3} (packing of cubes), and {5,3,3} (packing of dodecahedra) [11]. They correspond to $s = -1$, $s = -2$, and $s = 1$, respectively. Note that the case $s = 0$ does not correspond to any regular froth. Indeed, the only solution $s = 0$ of Eq. (3.15) with $\langle f\rangle$ and $\langle n\rangle_N < 6$ both being integers is $\langle f\rangle = 10$, $\langle n\rangle_N = 5$, which is not regular.

Consider Eq. (3.15) in the Euclidean case (i.e., $s = 2$). This equation gives a relationship between the average number of neighbors per cell ($\langle f\rangle$) in the 3D froth and the average number of edges per cell ($\langle n\rangle_N$) in the 2D spherical shell network

$$\langle f\rangle = 6 + \frac{8}{\langle n\rangle_N - 4}. \quad (4.1)$$

This equation gives the condition for the Euclidean space filling by a shell-structured-inflatable froth. Note that, from Eq. (4.1), the minimal number of faces per cell of such a froth is ten, since $\langle n\rangle_N < 6$. It is known that the minimal number of neighbors per cell is eight for an Euclidean froth. Thus an Euclidean froth with $8 \leqslant \langle n\rangle_N < 10$ necessarily contains local topological defects of the kind discussed in Appendix B..

Recall that the shell network is the superposition of two elliptic 2D froths, the ''incoming'' and the ''outgoing'' froths. The pattern of edges constituting the shell network sets the value of $\langle n\rangle_N$. Therefore Eq. (4.1) allows us to construct systematically 3D Euclidean shell-structured-inflatable froths starting from the 2D shell networks.

The simplest 2D froth is the hexagonal lattice. The examples displayed in Figs. 4, 5, and 6 illustrate the construction of ordered, monotiled 3D froths from a shell network generated by different superpositions [cf. Figs. 4(a), 5(a), and 6(a)] of two hexagonal lattices. Figures 4(b) and 4(c) show two 3D unit cells constructed from the network [4(a)] (see also [12]). The cell [4(b)] is topologically equivalent to Kelvin's α tetrakaidecahedron [7,8] (it builds up the Kelvin froth shown in Fig. 3), and the cell [4(c)], to its twisted variant [13]. Both structures have $\langle f\rangle = 14$ and $\langle n\rangle_N = 5$, i.e., $s = 0$ Eq. (3.15). They are indeed Euclidean space fillers.

Figure 5(a) shows part of a shell network with five-sided faces, generated by the superposition of two ''squeezed'' hexagonal lattices (see also [12]). Figures 5(b) and 5(c) show the 3D unit cells constructed from the network [5(a)]. These cells have again $\langle f\rangle = 14$. The unit cell [5(b)] is topologically equivalent to the β tetrakaidecahedron (the Williams cell [14]). It has $\langle n\rangle_N = 5$, and is an Euclidean space filler according to Eq. (3.15).

The unit cell of Fig. 5(c) is topologically equivalent to the 14-sided cell (the Goldberg cell [15]) which occurs, among others, in clathrates [8], in t.c.p. structures [16,17], and in the minimal froth of Weaire and Phelan [18]. The space can be filled layer by layer with Goldberg cells only. The layers (Fig. 5) are Euclidean and the network [5(a)] is the same as that of the Williams space filler. However, successive layers are more and more distorted [19], as shown in Fig. 5(d). This distortion, which stretches the network in one direction and compresses it in the other, strongly suggests that we are filling the hyperbolic 3D space with a stack of Euclidean layers. It is possible to prove this contention by filling the space shell by shell instead of layer by layer. When doing so, one finds that most of the shell network is composed of pentagons (12 out of 14 in each 3D cell), but a finite density of hexagons (2 out of 14 in each 3D cell) is needed in order to close a shell. Thus $\langle n\rangle_N > 5$ which, according to Eq. (3.15), implies $s > 2$. Hence the 3D manifold tiled by Goldberg cells is hyperbolic.

With another intersection of the two ''squeezed'' hexagonal lattices, one generates the shell network shown in Fig. 6(a). The corresponding 3D unit cell [6(b)] has $\langle f\rangle = 16$ (eight quadrilaterals, six hexagons, and two octagons) and $\langle n\rangle_N = 4.8$. As far as we know, this unit cell is a monotile Euclidean space filler.

Figure 7 shows an example of an Euclidean shell-structured-inflatable froth made of two different cells [8]. The shell network [7(a)] also has two different tiles. The associated 3D unit cell [7(b)] has $\langle f\rangle = 12$.

Any Euclidean shell-structured-inflatable froth made with topologically identical cells can be constructed from a shell network generated by superposition of two hexagonal lattices. The construction of 3D disordered froths from 2D disordered shell networks is discussed in Appendix C.

Although a construction of 3D froths layer by layer has been given in [12], it must be emphasized that our approach, combining spherical shells with the logistic map, is more general and provides a unifying way to deal with 3D space-filling structures, whether regular or not, whatever the curvature of the manifold which they are tiling.

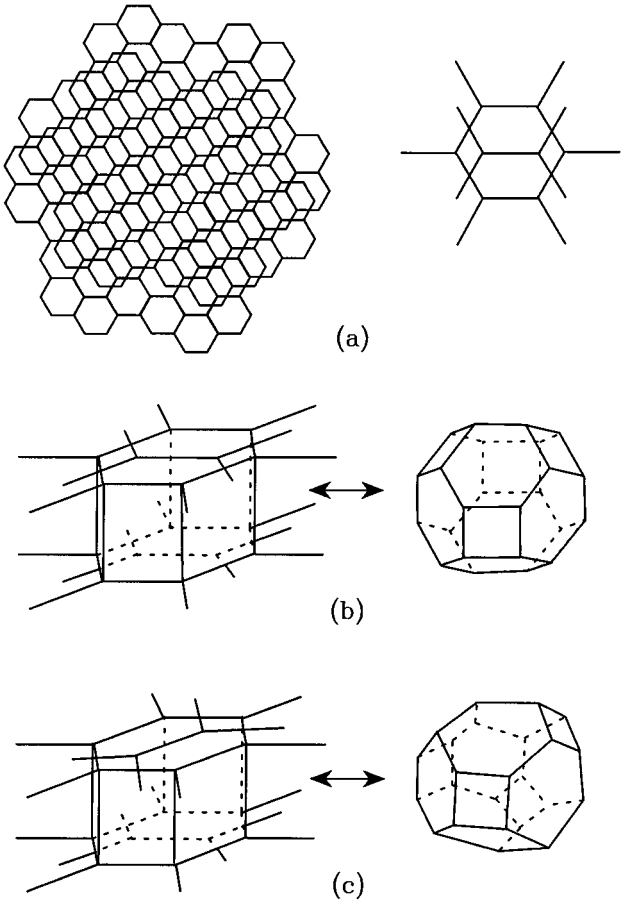

FIG. 4. The two 3D space-filling unit cells constructed from the shell network (a). The cell (b) is topologically equivalent to Kelvin's α tetrakaidecahedron and the cell (c) to its twisted variant. Both have 14 faces.

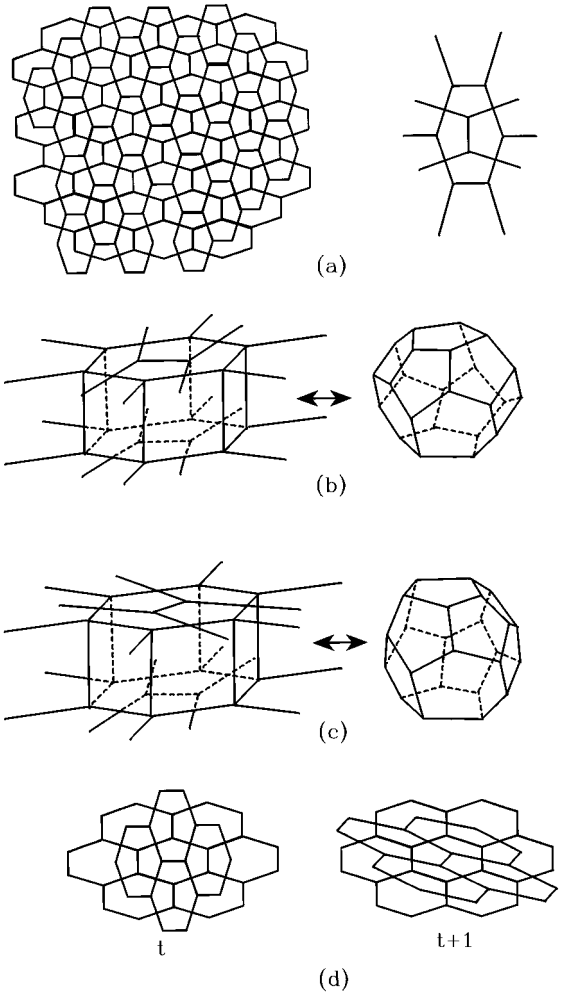

FIG. 5. The two 3D space-filling unit cells constructed from the shell network (a) generated by the superposition of two ''squeezed'' hexagonal lattices. The cell (b) is topologically equivalent to the β tetrakaidecahedron. The cell (c) is topologically equivalent to the Goldberg cell. (d) shows the distortion of the 2D cells in the successive shell networks resulting from filling with Euclidean layers of Goldberg cells a space which is hyperbolic.

V. BOUNDS ON TOPOLOGICAL PROPERTIES OF NATURAL CELLULAR SYSTEMS AND T.C.P. STRUCTURES

The average number ($\langle n\rangle$) of edges per face of a 3D froth is in general different from the average number of edges per face in the shell-network ($\langle n\rangle_N$). For example, the froths in Fig. 4 and 5(b) have $\langle n\rangle_N=5$ and $\langle n\rangle=5.14$, the froth in Fig. 6 has $\langle n\rangle_N=4.8$ and $\langle n\rangle=5.25$ and the froth in Fig. 7 has $\langle n\rangle_N=5.33$ and $\langle n\rangle=5$.

The value of $\langle n\rangle$ is related to the average number of faces per 3D cell by

$$\langle f\rangle=\frac{12}{6-\langle n\rangle}. \tag{5.1}$$

It is interesting to study the competition between Eq. (5.1) and the Euclidean space-filling condition given by Eq. (4.1). These two relations $\langle f\rangle(\langle n\rangle_N)$ (labeled ''space filling'') and $\langle f\rangle(\langle n\rangle)$ (labeled ''3D cell'') are plotted in Fig. 8. They meet at the point $(\langle n\rangle^*,\langle f\rangle^*)$ given by

$$(\langle n\rangle^*,\langle f\rangle^*)=\left(\frac{10+2\sqrt{7}}{3}\right), \tag{5.2}$$

It is only when the equality $\langle n\rangle=\langle n\rangle_N=\langle n\rangle^*$ (which corresponds to $\langle f\rangle^*=13.29\cdots$) is satisfied that an arbitrary cell has the freedom to adhere to a preexisting shell by any subset of its faces, without adjustment. This freedom grants, therefore, a larger number of possibilities for building up a froth and its maximizes the orientational entropy per cell. Indeed, Eq. (5.1) is a constraint on any single 3D cell, whereas Eq. (4.1) is a constraint on the set of 3D cells in a layer. When $\langle n\rangle=\langle n\rangle_N=\langle n\rangle^*$, one of the two constraints is automatically satisfied by the other and the orientational entropy is increased [20].

Note that the value $\langle f\rangle^*=13.29\cdots$ falls within the range of several already known bounds. It is consistent with the values 13.2 and $13.33\cdots$ resulting from the decurving of the dodecahedral packing with 14- and 18-sided cells or 14- and 16-sided cells, respectively [21]. Kusner [22] has shown that a single cell with minimal interfaces in a froth which is lo-

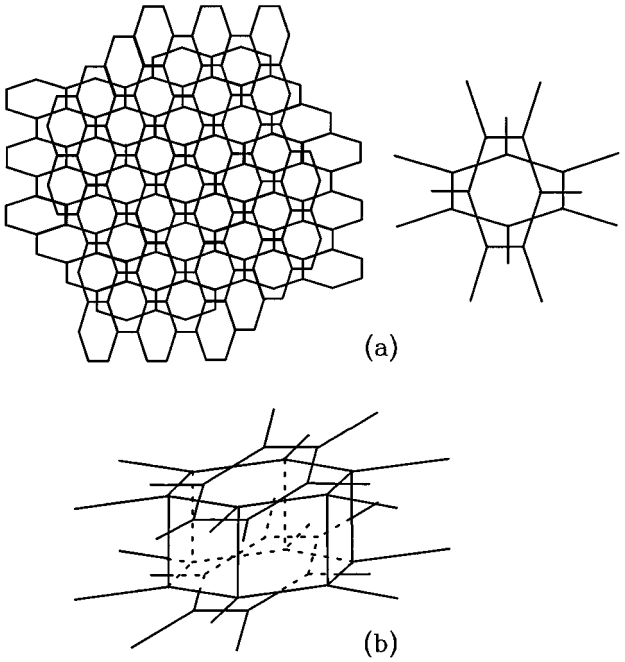

FIG. 6. The 3D space-filling unit cell (b) (which has 16 faces) resulting from the shell network (a) generated by the superposition of two ''squeezed'' hexagonal lattices.

cally Euclidean or hyperbolic cannot have less than 13.39 faces on average. It is also known that the minimal number of faces per cell of a periodic, monotiled froth is 14. Weaire and Phelan have recently given an example of froth with $\langle f\rangle = 13.5$ (the so-called $A15$ phase) which minimizes the total interfacial area [18] (see also [23]).

Natural froths minimize their free energy [(*configurational energy*) − (*temperature*) × (*entropy*)]. With the bounds given above, this condition is realized when the value of $\langle f\rangle$ is between $13.29\cdots$ and 13.5 (or 14 for periodic monotiled froths). The lower bound corresponds to configurations with a maximal orientational entropy, whereas the upper bound corresponds to configurations with a minimal interfacial energy.

There exists a class of natural structures, the Frank and Kasper phases (or the larger class of the t.c.p. structures [16,17]), for which $\langle f\rangle$ falls within these bounds. These structures are periodic and made of 12-, 14-, 15-, and 16-sided cells whose faces are either pentagons or hexagons. It can be verified that some of them fulfil the condition of Euclidean space filling given by Eq. (4.1). We can therefore assume that the t.c.p. structures are Euclidean shell-structured-inflatable froths. Then their shell network is a periodic tiling made of pentagons and hexagons only. Let the 2D unit cell of the shell network consist of $f^{(5)}$ pentagons and $f^{(6)}$ hexagons, belonging to N^* polyhedra within the layer between the two subsequent shells. The number of polyhedra in the 3D unit cell is a multiple of N^*. The average number of edges per face in the shell network is

$$\langle n\rangle_N = \frac{6f^{(6)} + 5f^{(5)}}{f^{(6)} + f^{(5)}}. \tag{5.3}$$

Substituting into Eq. (4.1), one obtains

$$\langle f\rangle = \frac{20f^{(6)} + 14f^{(5)}}{2f^{(6)} + f^{(5)}}. \tag{5.4}$$

The number of polyhedra in the 3D unit cell can be calculated with the help of the numbers of faces of the ''outgoing'' (f_+) and ''incoming'' (f_-) froths in the unit cell of the shell network. These numbers coincide with the numbers of polyhedra in the layers above (f_+) and below (f_-) the shell which have one or more faces belonging to the 2D unit cell. In the limit of large shell networks, one has the relation $v_{+(-)} \simeq 2f_{+(-)}$, with v_+ (respectively, v_-) counting the

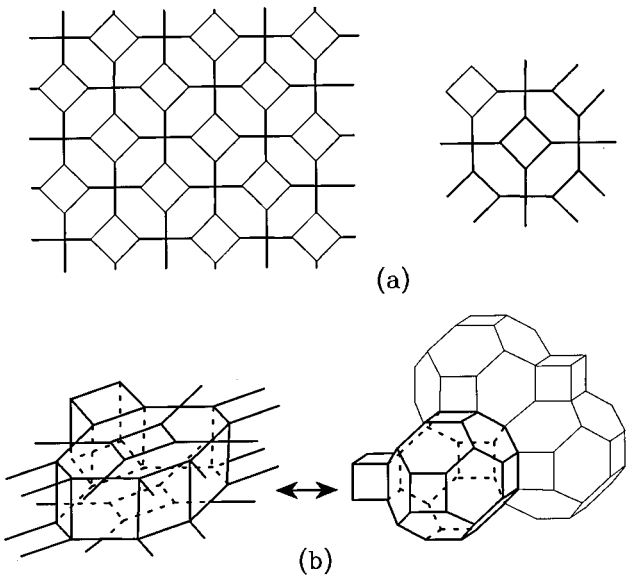

FIG. 7. Example of a 3D periodic shell-structured-inflatable froth (with $\langle f\rangle = 12$) whose unit cell has two different elementary cells. (a) Shell network. (b) 3D unit cell.

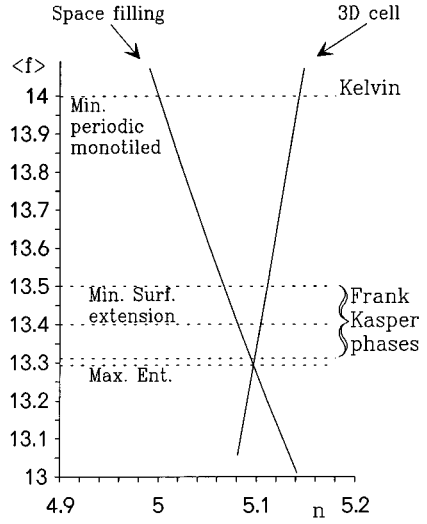

FIG. 8. The average number $\langle f\rangle$ of faces per cell in a froth plotted as a function of the average number $\langle n\rangle_N$ of edges per 2D cell in the shell network [Eq. (4.1), curve labeled ''space filling''] and of the average number $\langle n\rangle$ of edges per face in the froth [Eq. (5.1), curve labeled ''3D'']. The abscissa n represents both $\langle n\rangle_N$ and $\langle n\rangle$.

number of three-connected vertices in the 2D unit cell which belong to the ''outgoing'' (respectively, ''incoming'') froth. Equation (3.10) can then be written in terms of the quantities associated with the 2D unit cell only

$$f_+ + f_- = v_\times \left(\frac{\langle n \rangle_N - 4}{6 - \langle n \rangle_N} \right) \tag{5.5}$$

($v_\times$ counts the number of four-connected vertices in the 2D unit cell). On the other hand, since the 3D system is periodic, one has $f_+ + f_- = 2N^*$ on average. Therefore Eq. (5.5) can be written as

$$N^* = \frac{v_\times}{2} \left(1 + 2 \frac{f^{(6)}}{f^{(5)}} \right). \tag{5.6}$$

If one puts into Eq. (5.4) the simplest combinations of integers $f^{(5)}$ and $f^{(6)}$ which are such that $\langle f \rangle$ falls within the two bounds $13.29\cdots$ and 13.5, one retrieves the average number of faces of the 3D unit cell of all experimentally known t.c.p., which are listed in Table I. [The table gives all the possible combinations $(f^{(5)}, f^{(6)})$ up to $f^{(6)}=4$ and, for $f^{(6)} \geqslant 4$, only those corresponding to known natural structures.] Also given are the corresponding values of N^*, obtained from Eq. (5.6). These values of N^* are exactly equal to the sum of the lowest noncongruent numbers of 16-(p), 15-(q), 14-(r), and 12-sided polyhedra (x) in the structural formula of the corresponding t.c.p. [17]. The table presents also several simple combinations $(f^{(6)}, f^{(5)})$ which correspond to structures not (yet) observed (they are indicated by blanks in the last column). Notably, combinations (2,23) and $(2,25)\cdots$ may be good candidates for the t.c.p. structures yet to be observed. On the other hand, combinations (2,19), (3,28), (3,29), and (4,39) may be too distorted to qualify as t.c.p. structures. They may be realized with atoms of very different sizes. Note finally that when $\langle f \rangle$ is represented as a function of the ratio $f^{(5)}/f^{(6)}$, the structures in Table I tend to gather into distinct groups. This may indicate either the existence of unfavorable configurations or structural mode locking into the simplest t.c.p. structures ($A15$, $Z, \sigma, \ldots, C15$). All these facts strongly suggest that the t.c.p. are shell-structured-inflatable froths.

VI. CONCLUSION

In this paper we have introduced a way to study froths which emphasizes their shell structure. We have studied an important subclass of shell-structured froths, i.e., those which can be generated in a recursive way according to an inflationary procedure. For 2D froths (and networks with any coordination number) and 3D froths we have found that this recursive procedure is described by the logistic map. This map allows for a natural differentiation between froths tiling elliptic, hyperbolic, or Euclidean manifolds, without any *a priori* imposed curvature condition. In particular, the logistic map is able to characterize 3D curved manifolds, thereby providing a way to define the curvature from topological considerations when the Gauss-Bonnet theorem is not applicable. The logistic map in the 3D case enables us to recover known space-filling configurations, and also to suggest other ones. It is clear that the approach using the logistic map is very powerful, since classification of the 3D space-filling configurations is reduced to the study of the 2D tilings of the (elliptic) shell surface. As an example of the power and generality of this approach, we have been able to retrieve the topological properties of all experimentally known t.c.p. structures by studying the tiling of the shell surface by pentagons and hexagons.

ACKNOWLEDGMENTS

We are grateful to D. Weaire for many discussions. This work has been supported in part by the E.U. Human Capital and Mobility Program ''Physics of Foams,'' Ref. CHRX-CT-940542.

APPENDIX A: INFLATION OF TWO-DIMENSIONAL z-VALENT NETWORKS WITH $z \geqslant 4$

The generalization of Eq. (2.3) in the description of the 2D shell-structured-inflatable froths with coordination number $z \geqslant 4$ is as follows. Every shell has $(z-1)$ different types of vertices. Extending the notation of Sec. II, the various types of vertices are labeled by $V_a^{(t)}$, the number of vertices belonging to shell (t) from which $a=0,1,\ldots,z-2$, (respectively, $z-2-a$) edges are pointing towards the shell $(t+1)$ [respectively, shell $(t-1)$]. Every vertex $V_a^{(t)}$ adds a cells between shells (t) and $(t+1)$. The total number of cells $F^{(t)}$ between the two shells is

$$F^{(t)} = \sum_{a=0}^{z-2} a V_a^{(t)} = \sum_{a=0}^{z-2} (z-a-2) V_a^{(t+1)}. \tag{A1}$$

Let $\langle n \rangle$ denote the average number of edges per cell in the layer (t). If one sums over all cells in this layer, one obtains

$$\langle n \rangle F^{(t)} = \sum_{a=0}^{z-2} (a+1) V_a^{(t)} + \sum_{a=0}^{z-2} (z-a-1) V_a^{(t+1)}. \tag{A2}$$

Since

$$a+1 = \left(1 + \frac{1}{z-2} \right) a + \left(\frac{1}{z-2} \right) (z-a-2) \tag{A3}$$

and

$$z-a-1 = \left(1 + \frac{1}{z-2} \right) (z-a-2) + \left(\frac{1}{z-2} \right) a, \tag{A4}$$

one has

$$\begin{aligned} \langle n \rangle F^{(t)} = & \left(1 + \frac{1}{z-2} \right) \sum_{a=0}^{z-2} a V_a^{(t)} + \left(\frac{1}{z-2} \right) \sum_{a=0}^{z-2} (z-a-2) V_a^{(t)} \\ & + \left(\frac{1}{z-2} \right) \sum_{a=0}^{z-2} a V_a^{(t+1)} + \left(1 + \frac{1}{z-2} \right) \\ & \times \sum_{a=0}^{z-2} (z-a-2) V_a^{(t+1)} \\ = & \left(1 + \frac{1}{z-2} \right) F^{(t)} + \left(\frac{1}{z-2} \right) F^{(t-1)} + \left(\frac{1}{z-2} \right) F^{(t+1)} \\ & + \left(1 + \frac{1}{z-2} \right) F^{(t)}. \end{aligned} \tag{A5}$$

TABLE I. Average number of faces $\langle f \rangle$ and (minimal) number of elements in the 3D unit cell N^* of all the t.c.p. structures known experimentally (labeled in the last column) and of the hypothetical t.c.p. structures (indicated by a blank in the last column). The integers p, q, r, and x indicate, respectively, the proportions of 3D cells with 16, 15, 14, and 12 faces present in the 3D unit cell.

Number of hexagons	Number of pentagons	$\langle f \rangle$	N^*	p	q	r	x	t.c.p.
1	10	13.333 33	3	1	0	0	2	$C15$; $C14$
1	11	13.384 62	13	2	2	2	7	$p\sigma$; K_7Cs_6; μ; M
1	12	13.428 57	7	0	2	2	3	Z
2	24	13.428 57	14	1	2	5	6	P; δ
1	13	13.466 67	15	0	2	8	5	σ; H
1	14	13.5	4	0	0	3	1	$A15$
2	19	13.304 35	23					
2	21	13.36	25	6	2	2	15	C
2	23	13.407 41	27					
2	25	13.448 28	29					
2	27	13.483 87	31					
3	28	13.294 12	17					
3	29	13.314 29	35					
3	31	13.351 35	37	10	2	2	23	X
3	32	13.368 42	19	4	2	2	11	I
3	34	13.4	20					
3	35	13.414 63	41					
3	37	13.441 86	43					
3	38	13.454 55	11	0	2	5	4	J
3	40	13.478 26	23					
3	41	13.489 36	47					
4	39	13.319 15	47					
4	41	13.346 94	49					
4	43	13.372 55	51					
4	45	13.396 23	53	8	6	12	27	R
4	47	13.418 18	55	7	4	19	25	K^*
7	90	13.461 54	52	0	4	13	9	F
9	92	13.345 45	55	16	2	2	35	Mg_4Zn_7
11	142	13.463 41	41	7	4	19	25	K
13	136	13.358 02	81	20	6	6	49	T
13	136	13.358 02	81	23	0	9	49	SM
13	160	13.440 86	93	6	10	40	37	ν

One obtains finally the recursion relation

$$[\langle n \rangle (z-2) - 2(z-1)] F^{(t)} = F^{(t+1)} + F^{(t-1)}. \quad \text{(A6)}$$

The matrix form of this recursion relation is the same as for $z=3$ [Eq. (2.3)], with recursion parameter $s = \langle n \rangle (z-2) - 2(z-1)$. The initial conditions are $F^{(1)} = (z-2)\langle n \rangle$ and $F^{(0)} = 1$.

Euclidean tilings are associated with the fixed point $s^* = 2$, i.e., to the equation

$$\langle n \rangle = \frac{2z}{z-2}. \quad \text{(A7)}$$

The only regular solutions [z and $\langle n \rangle$ integers] of this equation are (6,3) (tiling by triangles), (4,4) (tiling by squares), and (3,6) (tiling by hexagons) [(dual of (6,3)].

APPENDIX B: NONINFLATABLE FROTHS

1. Noninflatable 2D froths

Some 2D shell-structured froths cannot be constructed according to the recursion procedure of Eq. (2.3). These froths have local inclusions which are topological defects in the recursion procedure. An inclusion in a layer is a cell with neighboring cells in this layer and only in one of the two neighboring layers. Topological defects fall in two classes: vertex decorations [Figs. 9(a) and 9(b)] and edge decorations [Fig. 9(c)]. In all cases the inclusion is on the + side of the shell (t).

Defects can be eliminated by removing one or more of the edges and their surrounding vertices. A vertex-decoration defect is then replaced by an ordinary vertex [Fig. 10(a)]. An edge-decoration defect is then replaced by edges on the shell [Fig. 10(b)].

The removal of one edge reduces by one unit the number of faces in the layer. This operation corresponds to the trans-

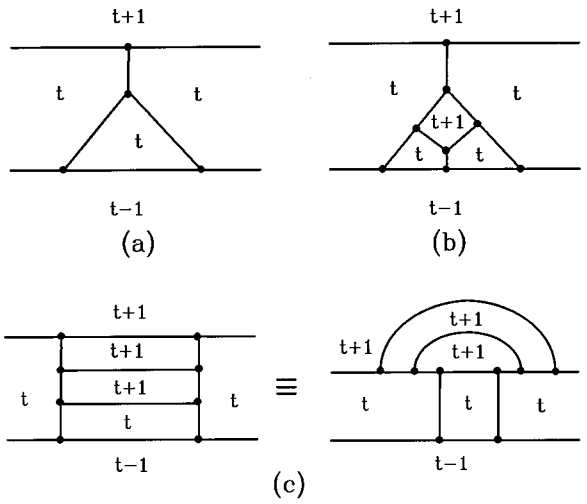

FIG. 9. Local topological defects in the 2D recursion procedure. (a) and (b) are examples of vertex decorations whereas (c) is an example of edge decoration. The index t denotes the topological distance.

formations $E\to E-3, V\to V-2, F\to F-1$. Consequently, since $\langle n\rangle = 2E/F$, the average number of edges per cell changes as

$$\langle n\rangle' = \langle n\rangle + \frac{1}{F-1}(\langle n\rangle - 6). \tag{B1}$$

The recursion parameter $s=\langle n\rangle - 4$ changes therefore as

$$s' = s + \frac{1}{F-1}(s-2). \tag{B2}$$

One sees that the fixed point $s^*=2$ remains unchanged by the defect elimination. Moreover, elliptic froths become more elliptic (i.e., $\langle n\rangle' < \langle n\rangle < 6$) whereas hyperbolic froths become more hyperbolic (i.e., $\langle n\rangle' > \langle n \gg 6$). Thus the Euclidean, hyperbolic, or elliptic character of the manifold tiled by the froth is not modified by the defect elimination (it is indeed given by the Euler-Poincaré characteristic which is a topological invariant).

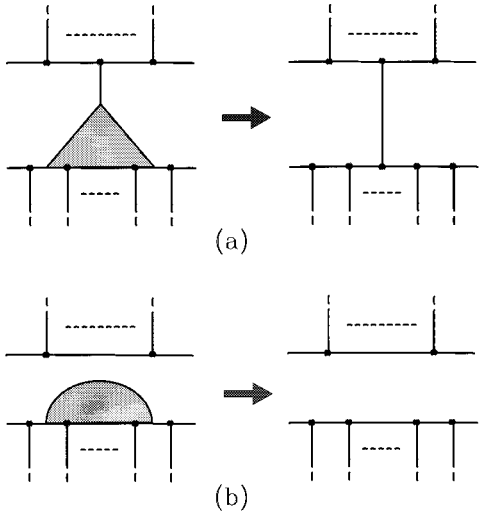

FIG. 10. Schematic representations of the elimination of a 2D local topological defect. (a) Vertex decoration. (b) Edge decoration.

2. Noninflatable 3D froths

By analogy with the 2D case, one can define a topological distance r between two cells A and B as the minimal number of faces that must be crossed by a path that connects A and B. A 3D shell-structured-inflatable froth is defined by the following two conditions:

(1) For any set of cells equidistant from a germ cell, there exists a closed non-self-intersecting surface that cuts these cells and no others.

(2) Any cell at the distance t from the germ cell is the neighbor of at least one cell at the distance $t+1$.

Shells are closed surfaces tiled by the faces of cells; they bound layers of equidistant cells. It is possible to connect two adjacent shells (t) and $(t+1)$ through a set of faces, each with one edge on shell (t) and one on shell $(t+1)$. Shell (t) separates the whole froth into an inner froth, constituted of cells at a distance $r \leqslant t$, and an outer froth, with cells at a distance $r > t$.

There are local defects which violate rules (1) or (2). These noninflatable configurations in the 3D froths are shown in Fig. 11. These are particular examples of the three general classes of the 3D topological defects: vertex, edge, and face decoration. As in 2D these noninflatable configuration can be eliminated. Defects elimination is made by removing one (or more) face(s), together with the surrounding edges and vertices. The removal of one face with n edges

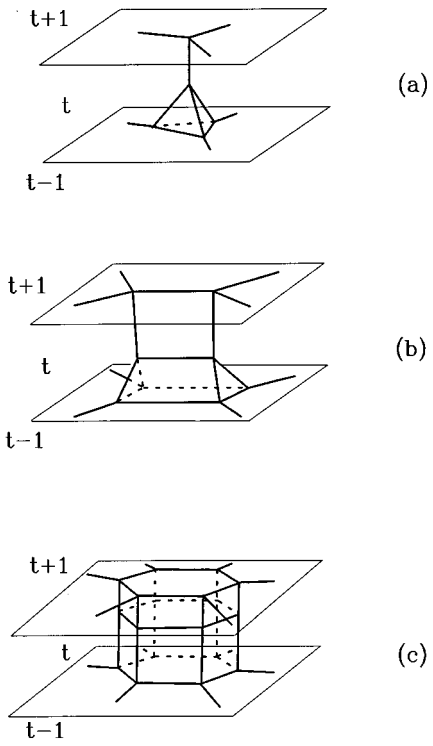

FIG. 11. Local topological defects in the 3D recursion procedure, (a) is a vertex decoration defect, (b) is an edge decoration defect, and (c) is a face decoration defect. The index t denotes the topological distance.

reduces by one unit the total number C of cells. This operation corresponds to the transformation $C \to C-1$ and $F \to F-1-n$. Consequently, since $\langle f \rangle = 2F/C$, the average number of faces per cell changes as

$$\langle f \rangle' = \langle f \rangle + \frac{1}{C-1}[\langle f \rangle - 2(n+1)]. \tag{B3}$$

In contrast to the 2D case, this transformation depends on the parameter n. This is not surprising since it is well known that in the 3D case the value of $\langle f \rangle$ is not directly related to the curvature of the manifold tiled by the froth.

APPENDIX C: RANDOM 3D EUCLIDEAN FROTHS FROM 2D RANDOM SHELL NETWORKS

Equation (4.1) implies that a 3D random froth can be constructed from the superposition of two 2D random froths. To study this general case it is useful to rewrite Eq. (4.1) in term of the number $p^{\times}$ of intersections of edges of the incoming froth by edges of the outgoing froth and vice versa. For a given shell (t) this quantity is equal to

$$p^{\times} = \frac{2V_{\times}^{(t)}}{E_{+}^{(t)} + E_{-}^{(t)}} = \frac{2}{3}\frac{2V_{\times}^{(t)}}{(V_{+}^{(t)} + V_{-}^{(t)})}, \tag{C1}$$

where we used the identity $3V_{+(-)}(t) = 2E_{+(-)}^{(t)}$. Using Eq. (3.10) it is possible to express $p^{\times}$ in terms of $\langle n \rangle_N$. One has

$$p^{\times} = \frac{2}{3}\left(\frac{6-\langle n \rangle_N}{\langle n \rangle_N - 4} - \frac{4\langle n \rangle_N}{(\langle n \rangle_N - 4)(V_{+}^{(t)} + V_{-}^{(t)})}\right). \tag{C2}$$

When the number of network cells is much larger than unity, one has $p^{\times} = (2/3)(6-\langle n \rangle_N)/(\langle n \rangle_N - 4)$. Substituting into (4.1), one obtains

$$\langle f \rangle = 10 + 6p^{\times}. \tag{C3}$$

In principle, in random froths, $p^{\times}$ can take any value between zero and infinity (but only between 2/3 and 1 for the periodic monotiled froths). For example, $p^{\times} = \infty$ corresponds to a froth made with layers of infinitely long bricks disposed, layer by layer, with orientation alternating by 90°. In this case the network is a square lattice. The opposite limit $(p^{\times} = 0)$ corresponds, for example, to a 3D froth made with layers of large and small cells, when the ratio between the cell sizes tends to infinity. In this case the network is the result of the superposition of a froth with cells of large sizes and a froth of small sizes and the probability of the intersection of edges of these two froths is vanishingly small.

[1] D. Weaire and N. Rivier, Contemp. Phys. **25**, 59 (1984).
[2] J. Stavans, Rep. Prog. Phys. **54**, 733 (1993).
[3] H. G. Schuster, *Deterministic Chaos* (Physik-Verlag, Weinheim, 1984).
[4] P. M. Oliveira, M. A. Continentino, and E. V. Anda, Phys. Rev. B **29**, 2808 (1984); B. K. Southern, A. A. Kumar, P. D. Loly, and M-A.S. Tremblay, Phys. Rev. B **27**, 1405 (1983); D. A. Lavis, B. W. Southern, and S. G. Davinson, J. Phys. C **18**, 1387 (1985).
[5] See, e.g., E. Kreyszig, *Differential Geometry* (Dover, New York, 1991).
[6] T. Aste and N. Rivier, J. Phys. A **28**, 1381 (1995).
[7] W. Thomson (Lord Kelvin) Philos. Mag. **24** (5), 503 (1887).
[8] R. Williams, *The Geometical Foundation of Natural Structure* (Dover, New York, 1979).
[9] B. R. Pollard, *An Introduction to Algebraic Topology* (University of Bristol Press, Bristol, 1977).
[10] S. S. Chern, Ann. Math. **45**, 747 (1944).
[11] H. M. S. Coxeter, *Regular Polytopes* (Dover, New York, 1973).
[12] J. A. Glazier and D. Weaire, Philos. Mag. Lett. **70**, 351 (1994).
[13] D. Weaire and R. Phelan, Philos. Mag. Lett. **69**, 107 (1994).
[14] R. E. Williams, Science **161**, 276 (1968).
[15] M. Goldberg, Tohoku Math. J. **40**, 226 (1934).
[16] F. C. Frank and J. S. Kasper, Acta Crystallogr. **12**, 483 (1959).
[17] D. P. Shoemaker and C. B. Shoemaker, Acta Crystallogr. Sect. B **42**, 3 (1986).
[18] D. Weaire and R. Phelan, Philos. Mag. Lett. **69**, 107 (1994).
[19] D. Weaire (private communication).
[20] N. Rivier and A. Lissowski, J. Phys. A **15**, L143 (1982).
[21] J. F. Sadoc and R. Mosseri, J. Phys. (Paris) **46**, 1809 (1985).
[22] R. Kusner, Proc. R. Soc. London. Ser. A **439**, 683 (1992).
[23] N. Rivier, Philos. Mag. Lett. **69**, 297 (1994).